Piebaldism and chromatophore development in reptiles is linked to the tfec gene Authors: Alan Garcia-Elfring¹, Christina E. Sabin^{2,3}, Anna L. Iouchmanov², Heather L. Roffey⁴, Sukhada P. Samudra², Aaron J. Alcala², Rida S. Osman², James D. Lauderdale^{3,5}, Andrew P. Hendry¹, Douglas B. Menke², and Rowan D. H. Barrett¹. ¹Department of Biology, Redpath Museum, McGill University, Montreal, QC, H3A 0G4, Canada ²Department of Genetics, University of Georgia, Athens, GA 30602, USA ³Neuroscience Division of the Biomedical and Translational Sciences Institute, University of Georgia, Athens, GA 30602, USA ⁴Biology Department, Vanier College, Montreal, QC, H4L 3X9, Canada ⁵Department of Cellular Biology, University of Georgia, Athens, GA 30602, USA

SUMMARY

Reptiles display great diversity in color and pattern; yet much of what we know about vertebrate coloration comes from classic model species such as the mouse and zebrafish. Captive-bred ball pythons (Python regius) exhibit a remarkable degree of color and pattern variation. A wide range of Mendelian color phenotypes are found in the pet trade, yet ball pythons remain an overlooked species in pigmentation research. Here, we investigate the genetic basis of the recessive piebald phenotype, a pattern defect characterized by patches of unpigmented skin (leucoderma). We performed whole-genome sequencing and used a casecontrol approach to discover a nonsense mutation in the gene encoding the transcription factor tfec, implicating this gene in the leucodermic patches in ball pythons. We functionally validated tfec in a lizard model (Anolis sagrei) using the gene editing CRISPR/Cas9 system and TEM imaging of skin. Our findings show that reading frame mutations in tfec affect coloration and lead to a loss of iridophores in Anolis, indicating that tfec is required for chromatophore development. This study highlights the value of captive-bred ball pythons as a model species for accelerating discoveries on the genetic basis of vertebrate coloration.

RESULTS AND DISCUSSION

46

47

48

49

50

51

52

53

54

55

56

57

58

59

60

61

62

63

64

65

66

67

68

69

70

71

72

73

Color variation is one of the most visually striking forms of biodiversity and has a long history of study in evolutionary biology, as it is easily observed and is often important for survival (1-3). Vertebrate color arises from pigments, structural coloration, and cell-cell interactions of three types of cells called chromatophores (4, 5). The skin of mammals and birds have only a single type of chromatophore, the melanocyte, which produces the brown pigment melanin. In contrast, reptiles and other poikilothermic vertebrates have melanophores which produce melanin, but also xanthophores and iridophores. Xanthophores contain yellow to orange pteridine pigments (6, 7), are called leucophores when they show a white color and erythrophores if they contain red carotenoid pigments (8, 9). Iridophores do not contain pigment, but instead have guanine crystals that act as reflective platelets to produce structural coloration (10). To date, the study of melanin-based pigmentation pathways has contributed the most to our understanding of pigmentation evolution and development in vertebrates (11). Moreover, a limited number of classic model species like the mouse and zebrafish dominate the literature on pigmentation biology (6, 12-25). Importantly, however, the knowledge gained from these models might not translate to other vertebrate groups like reptiles, which remain less studied (26 reviewed by 27). Ball pythons (Python regius), native to western sub-Saharan Africa and a popular snake in the international pet trade, present an excellent opportunity to study the genetic basis of vertebrate coloration in an emerging reptile model (28-30). Many Mendelian phenotypes ('base morphs'), representing rare, aberrant colorations (31-33), have been discovered in nature and propagated in captivity. Although ball python breeders have crossed these (inferred) single-gene color morphs to produce many more (inferred) multi-locus phenotypes ('designer morphs', Figure 1), the actual genetic basis of these phenotypes remains largely unknown (see references 28 and 29 for exceptions).

We investigated the genetic basis for a classic color morph found in the pet trade and common across a wide range of vertebrate taxa, the piebald. This phenotype is characterized by leucodermic patches and has been described by commercial breeders as recessive (34). Here, we analyze publicly available clutch data to investigate the mode of inheritance of the piebald

phenotype in ball pythons and use whole-genome sequencing and population genomics to identify the genomic region likely containing the causal mutation. Through the annotation of genetic variants (SNPs and indels), we identified a candidate causal mutation in a gene coding for a transcription factor. We functionally validated this locus in a squamate model using CRISPR/Cas9 gene editing and confirmed an effect on chromatophore development by TEM imaging.

Mode of inheritance and delineation of genomic region of interest

74

75

76

77

78

79

80

81

82

83

84

85

86

87

88

89

90

91

92

93

94

95

96

97

98

99

100

101

To test whether the piebald phenotype segregates as a simple Mendelian factor, we compiled 10 years' worth of clutch data from a commercial breeder (KINOVA). Consistent with the knowledge among commercial breeders, the proportion of piebald hatchlings indicates the piebald phenotype is inherited as a recessive Mendelian factor (Figure 2A). We applied wholegenome pool-seq to two sets of individuals, one set having the piebald phenotype and another set inferred by commercial breeders through pedigree analysis to not have the piebald mutation or mutations. We obtained an average read coverage of 50.5 and 52.6 for the piebald and non-piebald pools, respectively. To map SNPs showing high differentiation between pools to genes, we aligned reads to the annotated Burmese python (Python bivittatus) draft genome (Pmo2.0), from which we obtained 3,095,304 SNPs after filtering. Across all SNPs, we found an average F_{ST} of 0.03456 – indicating that population structure was successfully minimized. To delineate the genomic region of interest, we also mapped reads to a chromosome-length assembly. Using the draft assembly, we identified 129 fixed SNPs ($F_{ST} = 1.0$) and 369 SNPs with F_{ST} > 0.9 (Table S1). Indeed, the chromosome-length assembly shows a single region of high differentiation 8 Mb long on scaffold seven (7: 49526089–57612101), clearly delineating a genomic region of interest (Figure 2B).

Candidate genes and causal mutation

To obtain a list of candidate genes, we determined the gene annotations of variants with $F_{ST} > 0.90$ (Table S2). We used $F_{ST} > 0.90$ (rather than $F_{ST} = 1$) to account for factors that might preclude finding a fixed causal mutation (e.g., sequencing error, misidentification of a sample, or minor sample contamination, as multiple snakes are often housed together by commercial

breeders during breeding). We annotated SNPs for predicted loss-of-function to identify candidate causal mutations for the piebald phenotype. We found variants that mapped to the protein-coding sequences of 32 different genes. Most of the variants do not have a predicted effect on proteins, instead mapping to intronic and intergenic regions (344 'modifier' variants) and including one synonymous SNP (one 'low' impact mutation). The sole exception was a nonsense SNP (i.e., stop-gained mutation, 'high' impact) with F_{ST} = 0.96 located within the fifth coding exon of the *tfec* gene (NW_006534020.1 160458). On the chromosome length assembly, exon five spans 7: 52856864-52856924. This variant consists of a c.493C>T (p.Arg165*) mutation, resulting in a premature opal termination codon. This mutation is expected to result in a truncated protein with functional domains missing (e.g., basic helix-loop-helix on exon 7). The coverage of the reference and alternative alleles are 1X and 47X in the piebald pool and 46X and 0X non-piebald pool, respectively. The single read for the reference allele sequenced in the piebald pool resulted in a F_{ST} below 1.00, potentially due to sample misidentification or minor contamination from co-housed animals. Among non-piebald samples, the reference allele is fixed.

Deletion of a splice acceptor site in snakes

To examine sequence conservation around the candidate variant, we generated a multispecies sequence alignment of the *tfec* coding exon five and flanking intronic sequence. This alignment revealed the presence of a 4 bp deletion in snakes at an intron-exon junction relative to other vertebrates (Figure S2). Our analyses of RNA-seq data from the brown anole lizard (*Anolis sagrei*) demonstrate that this snake-specific deletion removes one of two alternative splice acceptor sites (i.e., 3' splice sites) that appear to be used in other squamates (Figure S3). We further note that certain other vertebrate species have single base pair changes that remove either splice site acceptor 1 (seen in some turtles) or splice site acceptor 2 (seen in some mammals, including humans). The use of splice acceptor 1 results in the inclusion of two additional codons relative to transcripts generated using splice acceptor 2. The functional differences, if any, between *tfec* proteins generated by the two different splice acceptors are unknown. However, we infer that ball pythons likely use the second acceptor site, which is

intact in ball pythons and other snakes. The stop codon mutation identified in piebald ball pythons occurs 6 bp from splice acceptor 2.

Targeted mutation of *tfec* in *Anolis* lizards

Protocols for genome editing in reptiles have been slow to develop because microinjection of single-cell embryos (zygotes) is difficult. To date, the brown anole lizard is the only squamate in which CRISPR/Cas9 has been successfully applied (35). Therefore, to functionally validate *tfec* as a gene with a role in reptile coloration, we generated lizards with reading frame disrupting mutations in *tfec* coding exon 5, successfully producing four F0 mutant individuals. *Mutant 1* carried one allele with a 56bp deletion and a second allele with a 1bp deletion, *Mutant 2* carried a 190 bp inversion and a 295 bp deletion, *Mutant 3* had a 4bp deletion, and *Mutant 4* had a 13bp insertion (Figure S4). These lizards all exhibited altered pigmentation phenotypes (Figure S5A-D).

Relative to lizards with normal pigmentation (Figure 3A), the four F0 *tfec* mutants showed reduced coloration, particularly in the snout, arms, and legs (Figure 3B; Figure S5). In this respect, the mutant phenotype is like the reduced pigmentation observed in piebald ball pythons. However, in contrast to ball pythons, the anole mutants have black eyes and lack the leucodermic patches characteristic of the piebald phenotype. Lateral and ventral views also revealed that the skin of *tfec* mutants is translucent, allowing the internal organs and ribs to become more visible. We noted that Mutant 1 displayed small patches of skin on its head that were wild type in appearance, suggesting the possibility of mosaicism this gene edited animal (Figure S5A). Therefore, we generated F1 lizards to examine pigmentation patterns *tfec* mutants that lack mosaicism. Crossbreeding mutant F0s together demonstrated that, just as in ball pythons, *tfec* is not required for viability or fertility in brown anoles in captivity. All F1 progeny (n=33) recapitulated the pigmentation phenotypes observed in the original F0 *tfec* mutants with no evidence of skin patches with wild type pigmentation (Figure S5E).

To further understand the phenotype caused by our induced mutations, we examined the eyes and skin of *tfec* and *tyrosinase* (*tyr*) brown anole mutants and compared them to wild-type individuals. The gene *tyrosinase* was chosen as an additional control for these comparisons

because of its role in melanin production. Through CRISPR/Cas9 editing we targeted *tyr* and generated a line of *tyr* mutants that carry an 8bp deletion in exon 2 of this gene. We dissected the eyes and skin from hatchlings homozygous for reading frame disrupting mutations in *tfec* or *tyr* (Figure 4, Figure S7). External examination of the eyes and skin revealed a loss of iridophores and presence of melanophores in *tfec*-/- F1 hatchlings. The loss of the iridescent iridophores make the eyes appear dark, much like the eyes of zebrafish that carry *tfec* mutations (36). In contrast, *tyr*-/- hatchlings retained iridophores but have an absence of melanophores. These changes in pigmentation were confirmed by transmission electron microscopy (TEM) on skin samples. In wild-type skin, TEM readily detected melanosomes and guanine crystals, which are characteristic features of melanophores and iridophores, respectively. In contrast, melanosomes were absent *from tyr*-/- skin and guanine crystals were absent from the skin of *tfec*-/- hatchlings.

A MiTF/TFE transcription factor linked to reptile coloration

The *tfec* gene encodes a transcription factor from the MiT-family of genes, which includes *mitf*, *tfe3*, *tfeb*, and *tfec*. These genes encode basic helix-loop-helix and leucine zipper functional domains and have important roles in lysosomal signaling, metabolism, and pigmentation (37, 38). *TFE3* and *TFEB* have pivotal roles lysosomal acidification and autophagy (39, 40), while *MITF*, *TFE3*, and *TFEB*, have all been linked to the development of cancer (37, 41, 42). *MITF* is also considered a master regulator of melanocyte development (41) and was first discovered through its association with Waardenburg syndrome type II (43), which is characterised by deafness, hypopigmentation, and microphthalmia (44). Mutations to *mitf* in mammals have been shown to affect melanocyte differentiation, resulting in apoptosis (45) and leucodermic patches (46, 47). One of the few studies investigating snake pigmentation identified a mutation in *mitf* in leucistic Texas rat snakes (33); this mutation, which results in an all-white phenotype, causes the loss of melanophores and xanthophores, but not iridophores.

Of the genes in the MiT-family, the function of *tfec* is the least well understood (48,49), but studies have shown that it is expressed, like *mitf*, in neural crest cells and retinal pigment epithelium of fish and mammals (50-52). In mouse and zebrafish models, *mitf* and *tfec* are

required for normal eye development (49, 50). Both *tfec* and *mitf* encode proteins with very similar helix-loop-helix domains (51), and it has been proposed that these two transcription factors regulate gene expression together as heterodimers (52). Kuiper et al. (2004) studied the expression patterns of MiT genes in human tissues and showed that *tfec* and *mitf* have multiple promoter regions and alternative splicing of functional domains, which may modulate target gene regulation (48). Interestingly, they found that *tfec* displays the broadest variety of functionally distinct isoforms, with differential spatiotemporal tissue distribution (e.g., spleen, kidney, bone marrow and small intestine). Although this study did not investigate the expression pattern in skin, the premature stop codon in the fifth exon of *tfec* found in piebald ball pythons is expected to result in a protein with missing basic helix-loop-helix and leucine zipper functional domains, likely disrupting target gene regulation (53). Our study adds *tfec* to the list of genes implicated in white spotting and pattern formation (54, 55).

tfec phenotypes in reptiles and other vertebrates

Identifying genes that affect color across a wide range of vertebrate species can lead to a deeper understanding of the mechanisms that underlie variation in color and pattern. Given the absence of iridophore and xanthophore cell types in mammals, it is particularly important to expand functional genetic studies of pigmentation beyond mice to better understand the biology of these chromatophore cell types. For example, while we found that *tfec* affects reptile color, a mouse study showed that *tfec* mutants have normal coat pigmentation (56), highlighting the need to study a wider range of taxa than traditional model organisms. Indeed, *tfec* was not included in a recent curated list of genes known to affect pigmentation (16). However, more recent work on zebrafish has shown that *tfec* is required for iridophore cell fate specification (64). Zebrafish *tfec* mutants also display delayed development of melanophores and xanthophores, but these chromatophores recover by day 4 post-fertilization. The *tfec*-associated phenotypes in reptiles and zebrafish, contrast with reported *mitf* phenotypes in these species. In zebrafish, mutations to *mitf* result in a loss of melanophores, a reduction in xanthophores, and an increase in iridophore density (57). In contrast, Texas rat snakes with a mutated *mitf* gene are leucistic (i.e., all-white), lacking melanophores and xanthophores but

showing no difference in iridophore density (33). Therefore, mutations in *tfec* and *mitf* produce distinct pigmentation phenotypes, with *tfec* being essential for iridophore development.

214

215

216

217

218

219

220

221

222

223

224

225

226

227

228

229

230

231

232

233

234

235

236

237

238

239

240

241

Our results support the conclusion that mutations to tfec in ball pythons cause piebaldism or white spotting, whereas in the brown anole they result in hypopigmentation and lack of iridophores. However, three main points remain unresolved. First is the question of what accounts for the species-specific differences in pigmentation phenotypes. It is known that ball pythons and lizards likely acquire their adult color pattern by different mechanisms (5). Ball pythons have a fixed pattern specified in the embryo, prior to hatching and scale development, and as adults they do not show scale-by-scale coloration. In contrast, many lizards exhibit scaleby-scale coloration that is specified between the juvenile and adult stage. Thus, differences in the timing of gene expression of chromatophores may play a role in the species-specific differences in pigmentation phenotypes. Also unresolved is whether piebald ball pythons have iridophores in either pigmented or white skin. In the Texas rat snake, white coloration arises with iridophores present (33). In the leopard gecko, skin from the ventral side is white but features a complete absence of all chromatophores (58). Since tfec is required for iridophore development in both the brown anole and zebrafish, the white patches in piebald ball pythons may lack all chromatophores. However, TEM imaging will be needed to confirm the chromatophore content of piebald skin in ball pythons. A third point that requires further study is the role of the splice site deletion we detected in snakes and the function of different TFEC protein isoforms across reptile taxa. The splice site deletion itself does not cause piebaldism, since it is present in wild type ball pythons and other snake species. However, the presence of two distinct splice acceptor sites is deeply conserved across many squamate reptiles, and our data demonstrate that both acceptor sites are used in anoles. Whether the ability to produce different TFEC isoforms contributes to species-specific differences in tfec function remains to be tested.

In summary, the finding of a nonsense mutation associated with the piebald phenotype in ball pythons in combination with targeted mutation and TEM imaging in a brown anole model shows *tfec* has an important role in reptile coloration. Mutations to *tfec* lead to

hypopigmentation and a loss of iridophores in the skin and eyes of brown anoles. In snakes, *tfec* is likely to be required for the development of chromatophores migrating to body regions that correspond to leucodermic patches observed in piebald ball pythons. Our work highlights the advantages of using ball pythons as a model organism and working with non-academic communities like reptile breeders to accelerate discoveries in pigmentation research in an under-studied class of vertebrates.

STAR*METHODS

Detailed methods are provided in the online version of this paper.

KEY RESOURCES TABLE

- Lead contact
- Materials availability
- o Data and code availability
 - RESOURCE AVAILABILITY
 - EXPERIMENTAL MODEL AND SUBJECT DETAILS
- METHOD DETAILS
 - Analysis of clutch data, sample collection, DNA extraction and sequencing
 - Bioinformatics
 - o Functional validation of the putative piebald mutation in *Anolis sagrei*
 - Dissection of eyes and TEM imaging of skin
- o Gene nomenclature

262

263

265

242

243

244

245

246

247

248

249

250251

252

254

255

257

258

259260

SUPPLEMENTAL INFORMATION

264 Supplemental information can be found online at: https://doi.org/

ACKNOWLEDGEMENTS

APH and RDHB were supported by NSERC Discovery Grants and Canada Research Chairs. ALI
and CES were supported by NIH training grant T32GM007103. Additional support came from an
NSF EDGE Program grant (#1827647) awarded to DBM and JDL. We thank Jose Avila-Cervantes
for his assistance with PCR.

270

AUTHOR CONTRIBUTIONS

271

286

288

289

290

291

292

293

294

272 AGE, APH, and RDHB conceived the study and its design, with contributions from JDL and DBM. HLR collected and catalogued shed skin samples. AGE performed DNA extractions and 273 274 bioinformatics to analyze whole-genome data. DBM and JDL carried-out CRISPR/Cas9 project oversight. CES performed in vitro test of tfec CRISPR gRNA, preparation of tfec RNP, tfec 275 276 surgeries/microinjection, breeding of tfec-/- lizards, eye & skin dissections and 277 stereomicroscope images, preparation of skin samples for TEM imaging and working with TEM microscopy technician. ALI performed egg collection, egg care, screening hatchlings for 278 279 phenotypes, documentation, and initial analysis of tfec phenotypes, genotyping, raising 280 hatchlings, and breeding tfec-/- lizards. SPS performed tfec surgeries/microinjections. AJA documented tfec phenotypes. RSO was instrumental in the creation of the tyrosinase mutant 281 282 line. JDL contributed with the analysis of tfec phenotypes, project oversight, project funding 283 (NSF EDGE grant). DBM performed tfec gene annotation, gRNA design, genotyping design, 284 analysis of tfec phenotypes, project oversight, project funding (NSF EDGE grant). AGE wrote the original draft with all authors contributing to review and editing. 285

DECLARATION OF INTERESTS

The authors declare no competing interests.

INCLUSION AND DIVERSITY

One or more of the authors of this paper self-identifies as an underrepresented ethnic minority in science. We also actively worked to promote gender balance in the list of references cited in this work. In our list of potential referees, we promoted diversity in scientific expertise, geographic location, career-stage, and gender.

REFERENCES

1. Caro, T. (2017). Wallace on Coloration: Contemporary Perspective and Unresolved Insights. Trends

295 Ecol Evol 32, 23-30. 10.1016/j.tree.2016.10.003.

- 296 2. Endler, J.A., and Mappes, J. (2017). The current and future state of animal coloration research. Philos
- 297 Trans R Soc Lond B Biol Sci 372. 10.1098/rstb.2016.0352.
- 3. Davison, A., Jackson, H.J., Murphy, E.W., and Reader, T. (2019). Discrete or indiscrete? Redefining the
- colour polymorphism of the land snail Cepaea nemoralis. Heredity 123, 162-175.
- 4. Patterson, L.B., and Parichy, D.M. (2013). Interactions with iridophores and the tissue environment
- required for patterning melanophores and xanthophores during zebrafish adult pigment stripe
- 302 formation. PLoS genetics 9, e1003561.
- 5. Jahanbakhsh, E., and Milinkovitch, M.C. (2022). Modeling convergent scale-by-scale skin color
- patterning in multiple species of lizards. Current Biology 32, 5069-5082. e5013.
- 305 6. Ziegler, I. (2003). The pteridine pathway in zebrafish: regulation and specification during the
- determination of neural crest cell-fate. Pigment Cell Res 16, 172-182. 10.1034/j.1600-
- 307 0749.2003.00044.x.
- 308 7. Andrade, P., and Carneiro, M. (2021). Pterin-based pigmentation in animals. Biol Lett 17, 20210221.
- 309 10.1098/rsbl.2021.0221.
- 8. Fang, W., Huang, J., Li, S., and Lu, J. (2022). Identification of pigment genes (melanin, carotenoid and
- 311 pteridine) associated with skin color variant in red tilapia using transcriptome analysis. Aquaculture 547,
- 312 737429.
- 313 9. Huang, D., Lewis, V.M., Foster, T.N., Toomey, M.B., Corbo, J.C., and Parichy, D.M. (2021).
- Development and genetics of red coloration in the zebrafish relative Danio albolineatus. Elife 10.
- 315 10.7554/eLife.70253.
- 316 10. Nicolaï, M.P., D' Alba, L., Goldenberg, J., Gansemans, Y., Van Nieuwerburgh, F., Clusella Trullas, S.,
- and Shawkey, M.D. (2021). Untangling the structural and molecular mechanisms underlying colour and
- 318 rapid colour change in a lizard, Agama atra. Molecular Ecology 30, 2262-2284.
- 11. McNamara, M.E., Rossi, V., Slater, T.S., Rogers, C.S., Ducrest, A.L., Dubey, S., and Roulin, A. (2021).
- 320 Decoding the Evolution of Melanin in Vertebrates. Trends Ecol Evol 36, 430-443.
- 321 10.1016/j.tree.2020.12.012.

- 12. Ishikawa, A., Sugiyama, M., Hondo, E., Kinoshita, K., and Yamagishi, Y. (2015). Development of a
- 323 novel pink-eyed dilution mouse model showing progressive darkening of the eyes and coat hair with
- 324 aging. Exp Anim 64, 207-220. 10.1538/expanim.14-0101.
- 325 13. Jackson, I.J. (1997). Homologous pigmentation mutations in human, mouse and other model
- 326 organisms. Hum Mol Genet 6, 1613-1624. 10.1093/hmg/6.10.1613.
- 327 14. Sturm, R.A. (2006). A golden age of human pigmentation genetics. Trends Genet 22, 464-468.
- 328 10.1016/j.tig.2006.06.010.
- 15. Tsetskhladze, Z.R., Canfield, V.A., Ang, K.C., Wentzel, S.M., Reid, K.P., Berg, A.S., Johnson, S.L.,
- 330 Kawakami, K., and Cheng, K.C. (2012). Functional assessment of human coding mutations affecting skin
- 331 pigmentation using zebrafish.
- 16. Baxter, L.L., Watkins-Chow, D.E., Pavan, W.J., and Loftus, S.K. (2019). A curated gene list for
- expanding the horizons of pigmentation biology. Pigment Cell Melanoma Res 32, 348-358.
- 334 10.1111/pcmr.12743.
- 17. Feng, Y., McQuillan, M.A., and Tishkoff, S.A. (2021). Evolutionary genetics of skin pigmentation in
- African populations. Hum Mol Genet 30, R88-R97. 10.1093/hmg/ddab007.
- 18. Ito, S., and Wakamatsu, K. (2011). Human hair melanins: what we have learned and have not learned
- from mouse coat color pigmentation. Pigment cell & melanoma research 24, 63-74.
- 339 19. Sturm, R.A. (2009). Molecular genetics of human pigmentation diversity. Human molecular genetics
- 340 18, R9-R17.
- 20. Adhikari, K., Mendoza-Revilla, J., Sohail, A., Fuentes-Guajardo, M., Lampert, J., Chacón-Duque, J.C.,
- Hurtado, M., Villegas, V., Granja, V., and Acuña-Alonzo, V. (2019). A GWAS in Latin Americans highlights
- the convergent evolution of lighter skin pigmentation in Eurasia. Nature communications 10, 1-16.
- 21. Phelps, G.B., Hagen, H.R., Amsterdam, A., and Lees, J.A. (2022). MITF deficiency accelerates GNAQ-
- driven uveal melanoma. Proceedings of the National Academy of Sciences 119, e2107006119.
- 22. Irion, U., and Nüsslein-Volhard, C. (2022). Developmental genetics with model organisms.
- Proceedings of the National Academy of Sciences 119, e2122148119.

- 348 23. Seruggia, D., Josa, S., Fernández, A., and Montoliu, L. (2021). The structure and function of the
- mouse tyrosinase locus. Pigment Cell & Melanoma Research 34, 212-221.
- 350 24. Logan, D.W., Burn, S.F., and Jackson, I.J. (2006). Regulation of pigmentation in zebrafish
- melanophores. Pigment cell research 19, 206-213.
- 352 25. Neuffer, S.J., and Cooper, C.D. (2022). Zebrafish Syndromic Albinism Models as Tools for
- 353 Understanding and Treating Pigment Cell Disease in Humans. Cancers 14, 1752.
- 354 26. Kuriyama, T., and Hasegawa, M. (2017). Embryonic developmental process governing the
- conspicuousness of body stripes and blue tail coloration in the lizard Plestiodon latiscutatus. Evolution &
- 356 development 19, 29-39.
- 357 27. Hasegawa, M., Kuriyama, T., Brandley, M., and Murakami, A. (2020). Blue, black, and stripes:
- 358 evolution and development of color production and pattern formation in lizards and snakes. Frontiers in
- 359 Ecology and Evolution 8, 232.
- 360 28. Brown, A.R., Comai, K., Mannino, D., McCullough, H., Donekal, Y., Meyers, H.C., Graves, C.W., Seidel,
- 361 H.S., and Consortium, B.W. (2022). A community-science approach identifies genetic variants associated
- with three color morphs in ball pythons (Python regius). Plos one 17, e0276376.
- 363 29. Dao, U.M., Lederer, I., Tabor, R.L., Shahid, B., Graves, C.W., and Seidel, H.S. (2022). Leucism and
- 364 stripe formation in ball pythons (Python regius) are associated with variants affecting endothelin
- 365 signaling. bioRxiv
- 30. Irizarry, K.J., and Bryden, R.L. (2016). In silico analysis of gene expression network components
- 367 underlying pigmentation phenotypes in the Python identified evolutionarily conserved clusters of
- transcription factor binding sites. Advances in bioinformatics 2016.
- 31. Borteiro, C., Diesel Abegg, A., Hirouki Oda, F., Cardozo, D.E., Kolenc, F., Etchandy, I., Bisaiz, I.,
- 370 Prigioni, C., and Baldo, J.D. (2021). Aberrant colouration in wild snakes: case study in Neotropical taxa
- and a review of terminology.
- 32. Iwanishi, S., Zaitsu, S., Shibata, H., and Nitasaka, E. (2018). An albino mutant of the Japanese rat
- 373 snake (Elaphe climacophora) carries a nonsense mutation in the tyrosinase gene. Genes & Genetic
- 374 Systems, 18-00021.

- 33. Ullate-Agote, A., and Tzika, A.C. (2021). Characterization of the leucistic Texas rat snake
- Pantherophis obsoletus. Frontiers in Ecology and Evolution 9, 583136.
- 34. Barker, D.G., and Barker, T.M. (2006). Ball pythons: the history, natural history, care and breeding
- 378 (VPI Library).
- 35. Rasys, A.M., Park, S., Ball, R.E., Alcala, A.J., Lauderdale, J.D., and Menke, D.B. (2019). CRISPR-Cas9
- gene editing in lizards through microinjection of unfertilized oocytes. Cell reports 28, 2288-2292. e2283.
- 36. Petratou, K., Spencer, S.A., Kelsh, R.N., and Lister, J.A. (2021). The MITF paralog tfec is required in
- 382 neural crest development for fate specification of the iridophore lineage from a multipotent pigment
- 383 cell progenitor. Plos one 16, e0244794.
- 384 37. Slade, L., and Pulinilkunnil, T. (2017). The MiTF/TFE family of transcription factors: master regulators
- of organelle signaling, metabolism, and stress adaptation. Molecular Cancer Research 15, 1637-1643.
- 38. Hejna, M., Moon, W.M., Cheng, J., Kawakami, A., Fisher, D.E., and Song, J.S. (2019). Local genomic
- features predict the distinct and overlapping binding patterns of the bHLH Zip family oncoproteins
- 388 MITF and MYC MAX. Pigment cell & melanoma research 32, 500-509.
- 39. Settembre, C., Di Malta, C., Polito, V.A., Arencibia, M.G., Vetrini, F., Erdin, S., Erdin, S.U., Huynh, T.,
- 390 Medina, D., and Colella, P. (2011). TFEB links autophagy to lysosomal biogenesis. science 332, 1429-
- 391 1433.
- 40. Martina, J.A., and Puertollano, R. (2017). TFEB and TFE3: the art of multi-tasking under stress
- conditions. Transcription 8, 48-54.
- 394 41. Levy, C., Khaled, M., and Fisher, D.E. (2006). MITF: master regulator of melanocyte development and
- melanoma oncogene. Trends in molecular medicine 12, 406-414.
- 42. Goding, C.R., and Arnheiter, H. (2019). MITF—the first 25 years. Genes & development 33, 983-1007.
- 397 43. Tassabehji, M., Newton, V.E., and Read, A.P. (1994). Waardenburg syndrome type 2 caused by
- mutations in the human microphthalmia (MITF) gene. Nature genetics 8, 251-255.
- 399 44. Steingrímsson, E., Moore, K.J., Lamoreux, M.L., Ferré-D'Amaré, A.R., Burley, S.K., Zimring, D.C.S.,
- 400 Skow, L.C., Hodgkinson, C.A., Arnheiter, H., and Copeland, N.G. (1994). Molecular basis of mouse

- 401 microphthalmia (mi) mutations helps explain their developmental and phenotypic consequences.
- 402 Nature genetics 8, 256-263.
- 403 45. Hu, S., Bai, S., Dai, Y., Yang, N., Li, J., Zhang, X., Wang, F., Zhao, B., Bao, G., and Chen, Y. (2021).
- 404 Deubiquitination of MITF-M Regulates Melanocytes Proliferation and Apoptosis. Frontiers in Molecular
- 405 Biosciences 8, 566.
- 46. Hauswirth, R., Haase, B., Blatter, M., Brooks, S.A., Burger, D., Drögemüller, C., Gerber, V., Henke, D.,
- Janda, J., and Jude, R. (2019). Correction: Mutations in MITF and PAX3 Cause "SplashedWhite" and
- 408 Other White Spotting Phenotypes in Horses. PLoS genetics 15, e1008321.
- 47. Baranowska Körberg, I., Sundström, E., Meadows, J.R., Rosengren Pielberg, G., Gustafson, U.,
- 410 Hedhammar, Å., Karlsson, E.K., Seddon, J., Söderberg, A., and Vilà, C. (2014). A simple repeat
- 411 polymorphism in the MITF-M promoter is a key regulator of white spotting in dogs. PLoS One 9,
- 412 e104363.
- 48. Lister, J.A., Lane, B.M., Nguyen, A., and Lunney, K. (2011). Embryonic expression of zebrafish MiT
- family genes tfe3b, tfeb, and tfec. Developmental Dynamics 240, 2529-2538.
- 49. Agostini, F., Agostinis, R., Medina, D.L., Bisaglia, M., Greggio, E., and Plotegher, N. (2022). The
- 416 Regulation of MiTF/TFE Transcription Factors Across Model Organisms: from Brain Physiology to
- 417 Implication for Neurodegeneration. Molecular Neurobiology, 1-24.
- 418 50. George, A., Zand, D.J., Hufnagel, R.B., Sharma, R., Sergeev, Y.V., Legare, J.M., Rice, G.M., Schwoerer,
- 419 J.A.S., Rius, M., and Tetri, L. (2016). Biallelic mutations in MITF cause coloboma, osteopetrosis,
- 420 microphthalmia, macrocephaly, albinism, and deafness. The American Journal of Human Genetics 99,
- 421 1388-1394.
- 422 51. Rowan, S., Chen, C.-M.A., Young, T.L., Fisher, D.E., and Cepko, C.L. (2004). Transdifferentiation of the
- retina into pigmented cells in ocular retardation mice defines a new function of the homeodomain gene
- 424 Chx10.
- 425 52. Bharti, K., Gasper, M., Ou, J., Brucato, M., Clore-Gronenborn, K., Pickel, J., and Arnheiter, H. (2012). A
- 426 regulatory loop involving PAX6, MITF, and WNT signaling controls retinal pigment epithelium
- 427 development. PLoS genetics 8, e1002757.

- 428 53. Kuiper, R.P., Schepens, M., Thijssen, J., Schoenmakers, E.F., and van Kessel, A.G. (2004). Regulation
- 429 of the MiTF/TFE bHLH LZ transcription factors through restricted spatial expression and alternative
- 430 splicing of functional domains. Nucleic acids research 32, 2315-2322.
- 431 54. Ahi, E.P., and Sefc, K.M. (2017). A gene expression study of dorso-ventrally restricted pigment
- 432 pattern in adult fins of Neolamprologus meeli, an African cichlid species. PeerJ 5, e2843.
- 433 55. Baxter, L.L., Hou, L., Loftus, S.K., and Pavan, W.J. (2004). Spotlight on spotted mice: a review of white
- 434 spotting mouse mutants and associated human pigmentation disorders. Pigment Cell Research 17, 215-
- 435 224.
- 436 56. Steingrímsson, E., Tessarollo, L., Pathak, B., Hou, L., Arnheiter, H., Copeland, N.G., and Jenkins, N.A.
- 437 (2002). Mitf and Tfe3, two members of the Mitf-Tfe family of bHLH-Zip transcription factors, have
- 438 important but functionally redundant roles in osteoclast development. Proceedings of the National
- 439 Academy of Sciences 99, 4477-4482.
- 440 57. Lister, J.A., Robertson, C.P., Lepage, T., Johnson, S.L., and Raible, D.W. (1999). Nacre encodes a
- 441 zebrafish microphthalmia-related protein that regulates neural-crest-derived pigment cell fate.
- 442 Development 126, 3757-3767.
- 443 58. Szydłowski, P., Madej, J.P., and Mazurkiewicz Kania, M. (2016). Ultrastructure and distribution of
- chromatophores in the skin of the leopard gecko (E ublepharis macularius). Acta Zoologica 97, 370-375.
- 59. Kofler, R., Orozco-terWengel, P., De Maio, N., Pandey, R.V., Nolte, V., Futschik, A., Kosiol, C., and
- 446 Schlötterer, C. (2011). PoPoolation: a toolbox for population genetic analysis of next generation
- sequencing data from pooled individuals. PloS one 6, e15925.
- 448 60. Castoe, T.A., De Koning, A.J., Hall, K.T., Card, D.C., Schield, D.R., Fujita, M.K., Ruggiero, R.P., Degner,
- J.F., Daza, J.M., and Gu, W. (2013). The Burmese python genome reveals the molecular basis for extreme
- adaptation in snakes. Proceedings of the National Academy of Sciences 110, 20645-20650.
- 451 61. Sedlazeck, F.J., Rescheneder, P., and Von Haeseler, A. (2013). NextGenMap: fast and accurate read
- 452 mapping in highly polymorphic genomes. Bioinformatics 29, 2790-2791.
- 453 62. Li, H., Handsaker, B., Wysoker, A., Fennell, T., Ruan, J., Homer, N., Marth, G., Abecasis, G., and
- Durbin, R. (2009). The sequence alignment/map format and SAMtools. Bioinformatics 25, 2078-2079.

- 455 63. Wysoker, A., Tibbetts, K., and Fennell, T. (2013). Picard tools version 1.90. Available online at picard.
- 456 sourceforge. net.
- 457 64. Kofler, R., Pandey, R.V., and Schlötterer, C. (2011). PoPoolation2: identifying differentiation between
- 458 populations using sequencing of pooled DNA samples (Pool-Seq). Bioinformatics 27, 3435-3436.
- 459 65. Dudchenko, O., Batra, S.S., Omer, A.D., Nyquist, S.K., Hoeger, M., Durand, N.C., Shamim, M.S.,
- 460 Machol, I., Lander, E.S., and Aiden, A.P. (2017). De novo assembly of the Aedes aegypti genome using Hi-
- 461 C yields chromosome-length scaffolds. Science 356, 92-95.
- 462 66. Dudchenko, O., Shamim, M.S., Batra, S.S., Durand, N.C., Musial, N.T., Mostofa, R., Pham, M., St
- 463 Hilaire, B.G., Yao, W., and Stamenova, E. (2018). The Juicebox Assembly Tools module facilitates de novo
- assembly of mammalian genomes with chromosome-length scaffolds for under \$1000. BioRxiv, 254797.
- 465 67. Chong, J.X., Buckingham, K.J., Jhangiani, S.N., Boehm, C., Sobreira, N., Smith, J.D., Harrell, T.M.,
- 466 McMillin, M.J., Wiszniewski, W., and Gambin, T. (2015). The genetic basis of Mendelian phenotypes:
- discoveries, challenges, and opportunities. The American Journal of Human Genetics 97, 199-215.
- 468 68. Cingolani, P., Platts, A., Wang, L.L., Coon, M., Nguyen, T., Wang, L., Land, S.J., Lu, X., and Ruden, D.M.
- 469 (2012). A program for annotating and predicting the effects of single nucleotide polymorphisms, SnpEff:
- 470 SNPs in the genome of Drosophila melanogaster strain w1118; iso-2; iso-3. Fly 6, 80-92.
- 471 69. Geneva, A.J., Park, S., Bock, D., de Mello, P., Sarigol, F., Tollis, M., Donihue, C., Reynolds, R.G., Feiner,
- 472 N., and Rasys, A. (2021). Chromosome-scale genome assembly of the brown anole (Anolis sagrei), a
- 473 model species for evolution and ecology. bioRxiv.
- 474 70. Concordet, J.-P., and Haeussler, M. (2018). CRISPOR: intuitive guide selection for CRISPR/Cas9
- 475 genome editing experiments and screens. Nucleic acids research 46, W242-W245.
- 476 71. Mehravar, M., Shirazi, A., Nazari, M., and Banan, M. (2019). Mosaicism in CRISPR/Cas9-mediated
- 477 genome editing. Developmental biology 445, 156-162.
- 478 72. Lewis, A.C., Rankin, K.J., Pask, A.J., and Stuart Fox, D. (2017). Stress induced changes in color
- expression mediated by iridophores in a polymorphic lizard. Ecology and Evolution 7, 8262-8272.
- 480 73. Reynolds, E.S. (1963). The use of lead citrate at high pH as an electron-opaque stain in electron
- 481 microscopy. The Journal of cell biology 17, 208.

482 STAR*METHODS 483 484 **RESOURCE AVAILABILITY Lead contact** 485 486 Further information should be directed to lead contact Alan Garcia-Elfring (alan.garcia-487 elfring@mail.mcgill.ca) or corresponding author Rowan Barrett (rowan.barrett@mcgill.ca). 488 **Data and code Availability** 489 Raw sequence data will be deposited in the sequence read archive (SRA) and processed data to 490 Dryad. All the code will be made available in a repository that mints DOIs or included in the supplemental information. 491 492 **METHOD DETAILS** 493 Analysis of clutch data, sample collection, DNA extraction and sequencing 494 495 To test whether the piebald phenotype segregates as a simple Mendelian factor, we compiled 496 10 years' worth of clutch data available online data from a commercial breeder (KINOVA). We 497 included data from piebald relevant crosses (https://kinovareptiles.com/incubator/?clutch_id=piebald): piebald vs. inferred non piebald, 498 499 piebald vs. inferred heterozygotes, and crosses between inferred heterozygotes. We obtained 500 ball python samples (shed skin) by appealing to commercial breeders from Canada (Mutation Creation, T. Dot Exotics, The Ball Room Canada, Designing Morphs). We used a case-control 501 approach, using shed skin samples from 47 piebald individuals (inferred to be homozygous for 502 503 the piebald variant; Table S3) and 52 non-piebald individuals (inferred to be homozygous wild-504 type from pedigrees; Table S4). Although individuals from both sets of samples contained

additional mutations (i.e., other base morphs), the only consistent difference between the two

pools was the piebald versus non-piebald phenotype difference. We attempted to maximize the

505

506

number of individuals that came from different families to minimize the effects of population structure, although there were some exceptions (Table S4). From each sample, we used approximately 0.1 g of shed skin, cut to small pieces using scissors, for DNA extraction. We extracted DNA following a standard phenol-chloroform procedure, with the modification of a 24-hour proteinase-K incubation time at 37 °C. Piebald and non-piebald samples were prepared on different working days to avoid contamination. We quantified all samples using a Picogreen® ds DNA assay (Thermo Fisher Scientific, Waltham, USA) on an Infinite® 200 Nanoquant (Tecan Group Ltd. Männedorf, Switzerland). After DNA extraction, we mixed DNA of individuals (according to phenotype) in equimolar amounts to obtain a single pool for each phenotype, 'piebald' and 'non-piebald.' Because extracted DNA from shed skin was degraded, we used PCR-based whole-genome libraries for both pools. We sequenced 150 bp pair-end reads on two lanes of Illumina HiSeqX. Library preparation and DNA sequencing were done at the McGill University and Genome Quebec Innovation Center in Montreal, Canada. The locus of interest was validated with PCR and Sanger sequencing.

Bioinformatics

We processed raw reads by filtering for read quality and length with the program *Popoolation* (59). We kept reads with a minimum quality of 20 (--quality-threshold 20) and a length of 50 bp (--min-length 50). We then aligned processed reads to the Burmese python (*Python bivittatus*) draft assembly Pmo2.0 (60) using the program *NextGenMap* (61). *NextGenMap* was designed for aligning reads to highly polymorphic genomes or genomes of closely related species. We used *SAMtools* (62) to convert SAM files to BAM format and remove reads with mapping quality below 20 (samtools view -q 20). PCR duplicates were removed with the program *MarkDuplicates* of *Picard Tools* (63). We used the *Popoolation2* (64) protocol to produce a sync file, which contains read counts for all nucleotides sequenced in the genome and used this for subsequent downstream analyses (e.g., F_{ST} scan). In a separate analysis, we applied the same protocol as above but instead aligned reads to the chromosome-length Burmese python reference genome, Python molurus bivittatus-5.0.2 HiC.assembly (65, 66).

We applied a genome-wide F_{ST} scan to search for SNPs showing high differentiation between the two pools. For this procedure, we used the *fst-sliding.pl* script of *Popoolation2* (-min-count 10, --min-coverage 20, --max-coverage 500, --min-covered-fraction 0, --window-size 1, --step-size 1, --pool-size 47:52, --suppress-noninformative). We then identified SNPs with high F_{ST} estimates (F_{ST} = 0.9-1.0) and mapped them to genes. We used a custom script to map SNPs with high differentiation to genes in the gene annotation file using the scaffold name and SNP position. Because the draft assembly of the Burmese python is highly fragmented (60), we also applied the same F_{ST} scan on data aligned to the chromosome-length genome assembly (65, 66) – thus obtaining better delineation of the genomic region of interest. However, this latter assembly is not annotated with genetic features, hence necessitating the use of both assemblies.

Mendelian phenotypes arise predominately due to mutations to the protein-coding sequences of genes (67). We thus annotated variants (SNPs and indels) with the software *snpEff* (68) to aid in identifying the putative causal mutation for the piebald phenotype within protein-coding genes. *SnpEff* was designed for annotating and predicting loss or reduced function effects of variants on gene protein-products, such as amino acid changes. This program provides an assessment of the impact of a variant, including 'HIGH' (e.g., stop codon), 'MODERATE' (e.g., non-synonymous change), 'LOW' (e.g., synonymous change), or 'MODIFIER' (change in an intergenic area).

Functional validation of the putative piebald mutation in Anolis sagrei

Gene editing was performed on wild-caught brown anole females under the approval and oversight of the University of Georgia Institutional Animal Care and Use Committee (A2019 07-016-Y3-A3). All experiments followed the National Research Council's Guide for the Care and Use of Laboratory Animals. CRISPR/Cas9 genome editing was carried out as previously reported (35) with the following modifications: For analgesia, rimadyl ($4\mu g/g$) was substituted for meloxicam, and the Cas9 RNP concentration was increased to 10 μ M. Cas9 RNP was produced by mixing SpCas9 2NLS with sgRNA (Synthego Corp, Menlo Park, CA) in 10 mM Tris-HCl, pH 7.4. In addition, Cas9 RNP was injected into a maximum of three follicles per ovary, prioritizing the

largest follicles. The size of follicles injected ranged from 1mm to 10mm in diameter, and included both previtellogenic and large, yolky follicles. Potential guide sites were obtained using *tfec* coding exon 5 from the *A. sagrei* AnoSag2.1 assembly (69), and targets were chosen using CRISPOR 4.4 (70), selecting targets with Fusi-Scores of 50% or greater. Before performing oocyte injections, we tested the ability of the Cas9 RNP to digest a PCR product than spans the target site. An equal mixture of two sgRNA was used to create *tfec* Cas9 RNP: Targets sites 5' AGAAACAGATACACGAGCAA 3' and 5' AGATACACGAGCAATGGCAA 3'. A total of 44 follicles in 12 adult females were injected to generate four *tfec* mutants. For the production of the *tyr* mutant line, a single sgRNA directed against *tyr* exon 2 was used to create *tyr* Cas9 RNP: Target site 5'ATGATAAAGGGAGGACACCT.

Eggs from CRISPR injected females were collected and incubated at 29°C. Upon hatching, lizard tail clips were collected, and genomic DNA prepared. Hatchlings were screened for mutations in tfec coding exon 5 by performing Sanger Sequencing on two different PCR amplicons: 466bp tfec amplicon (Tfec-F3: 5'-AAGGGCACATGGCTTGGAAG-3' and Tfec-R3: 5'-CAGTGGGTCTATACTAAACCTGA-3'); 1595bp tfec amplicon (Tfec-468-F: 5'-CCATGTACCATTTATCAATGCTATGC-3' and Tfec-1121-R: 5'-CATCGAATTGTTGCCAATCTGTG-3'). Sanger sequencing revealed mutations in two male (Mutant 1 and Mutant 3) and two female (Mutant 2 and Mutant 4) hatchlings. Mutant 1 and mutant 2 carried mutant alleles with large size differences that allowed us to gel purify two distinct PCR bands of different sizes from each lizard. We sequenced these gel purified bands to obtain clean chromatograms and verify the sequence of the mutant alleles. All mutations shifted the tfec reading frame and no evidence of wild-type alleles was detected in the mutants. To test for germline transmission, Mutant 1 was crossed with Mutant 2 and Mutant 4. Mutations in tyr were identified as previously described (35). We note that in many vertebrates, F0 genome edited individuals are highly mosaic (71). Injecting Cas9 RNP into immature lizard oocytes that are not fertilized for days to weeks allows for an extended period for Cas9 RNP to enter the nucleus and cut the target site on the maternal allele (and upon fertilization) the paternal allele. We speculate that may account for the low mosaicism that we observed in the F0 mutants.

Dissection of eyes and TEM imaging of skin

590

591

592

593

594

595

596

597

598

599

600

601

602

603

604

605

606

607

608

609

610

611

612

613

614

615

F0 tfec mutants were crossed to generate F1 tfec-/- progeny that we used for more detailed analyses of eyes and skin. An F0 tyr mutant male heterozygous for an 8bp deletion in tyr exon 2 was crossed to produce heterozygous F1 lizards; F1 tyr-/+ lizards were then intercrossed to produce F2 tyr-/- lizards. Wild-type, tyr-/-, and tfec -/- hatchlings were euthanized, and their eyes and skin from the trunk were collected immediately. The freshly dissected tissue was imaged using a ZEISS Discovery V12 SteREO microscope, AxioCam (MRc5), and Axio Vision 4.8.2 (release 06-2010). Electron microscopy was performed following the protocol of Lewis et al. (2017, reference 72) with modification. Samples were fixed in 2.5% glutaraldehyde in phosphate-buffered saline (PBS) overnight at room temperature. Fixed tissue samples were rinsed three times in PBS for 10 min each, before being dehydrated in increasing concentrations of ethanol consisting of 25%, 50%, 70%, 80%, 90%, 100%, and 100% anhydrous ethanol for 60 min each. Following dehydration, the cells were infiltrated with increasing concentrations of LR White resin in ethanol consisting of 25%, 50%, 75%, and 100% resin for 6 hr each step. After a second change of 100% resin, the samples were embedded in fresh resin in gelatin capsules. The gelatin capsules were capped to exclude air and the resin polymerized in an oven at 60°C for 24 h. The embedded tissues in resin blocks were sectioned with a diamond knife on a Leica Ultracut S microtome and ultrathin sections (60-70 nm) were collected onto formvar-coated 100 mesh hexagonal copper grids. The sections on grids were sequentially stained with 2% aqueous uranyl acetate for 30 min and Reynolds Lead Citrate for 8 min (73) and viewed in JEOL JEM-1011 transmission electron microscope at 80-100 kV. Images were captured with an AMT XR80M Wide-Angle Multi-Discipline Mid-Mount CCD digital camera, at a resolution of 3296 x 2460 pixels.

Gene nomenclature

Throughout this article, we follow gene nomenclature established in humans and zebrafish. In humans, gene names are capitalized (e.g., *TFEC* and *MITF*), whereas when referring to genes in

- other model organisms (e.g., zebrafish, mouse, and reptiles) the gene names are presented in
- 617 lowercase letters (e.g., *tfec* and *mitf*) for simplicity.

618

FIGURES

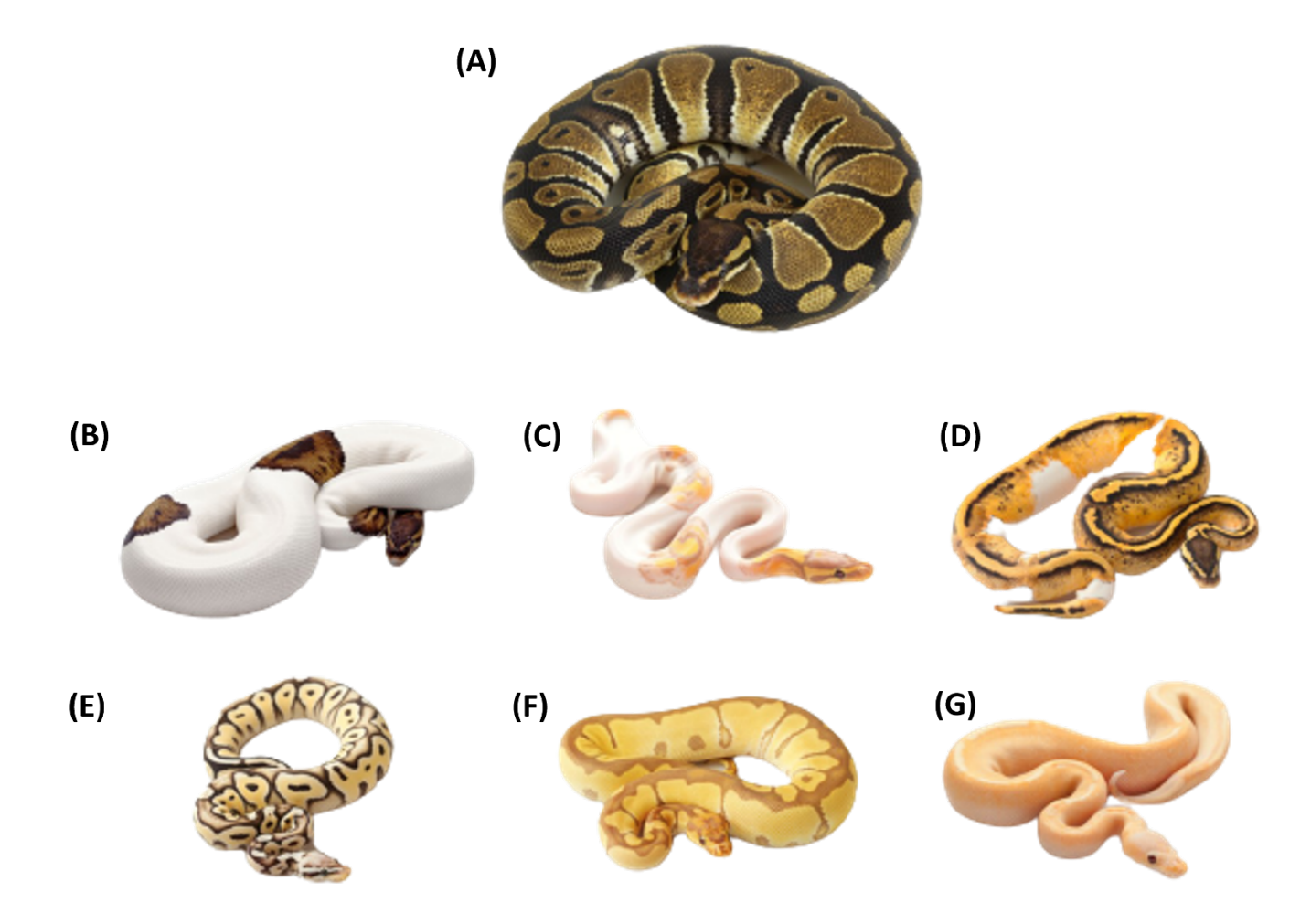


Figure 1. A small sample of the phenotypic variation found in captive-bred ball pythons (*Python regius*). (A) wild type, (B) piebald, (C) banana piebald, (D) pastel piebald, (E) pastel HRA enhancer, (F) ultramel clown, (G) banana champagne. Photo credit: pethelpful.com (A) and *Designing Morphs* (B-G).

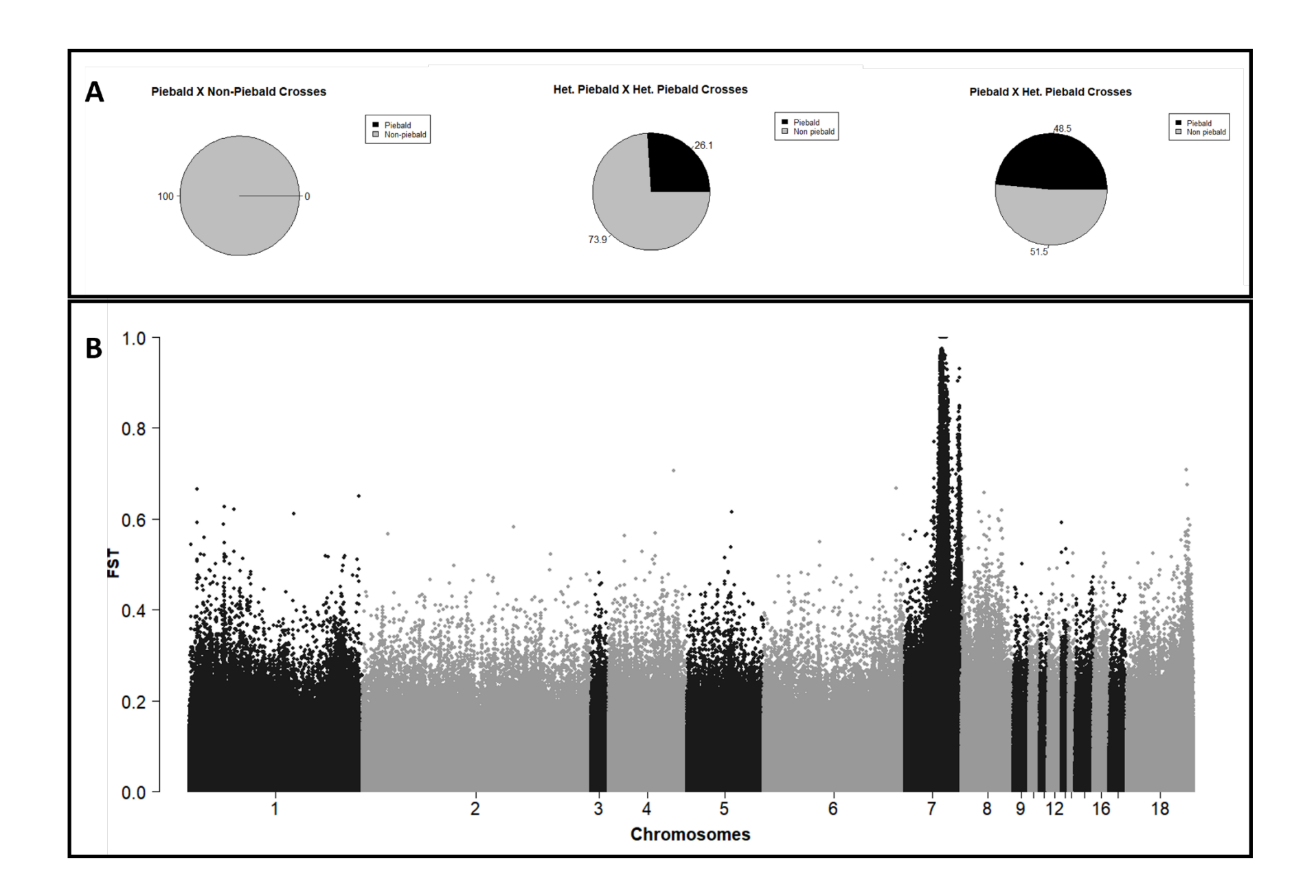


Figure 2. (A) Clutch records (2008-2018) from a commercial breeder (*KINOVA*) indicates piebald has a recessive mode of inheritance. Piebald vs. inferred non-piebald crosses: zero piebald hatchlings (P) and 311 non-piebald hatchlings (NP); Inferred heterozygote crosses: 60 P and 170 NP; Piebald vs. inferred heterozygote crosses: 238 P and 253 NP. (B) F_{ST} plot between piebald and non-piebald samples using a chromosome-length genome assembly. The F_{ST} peak on chromosome 7 delineates the region of interest containing the putative causal gene for the piebald phenotype.

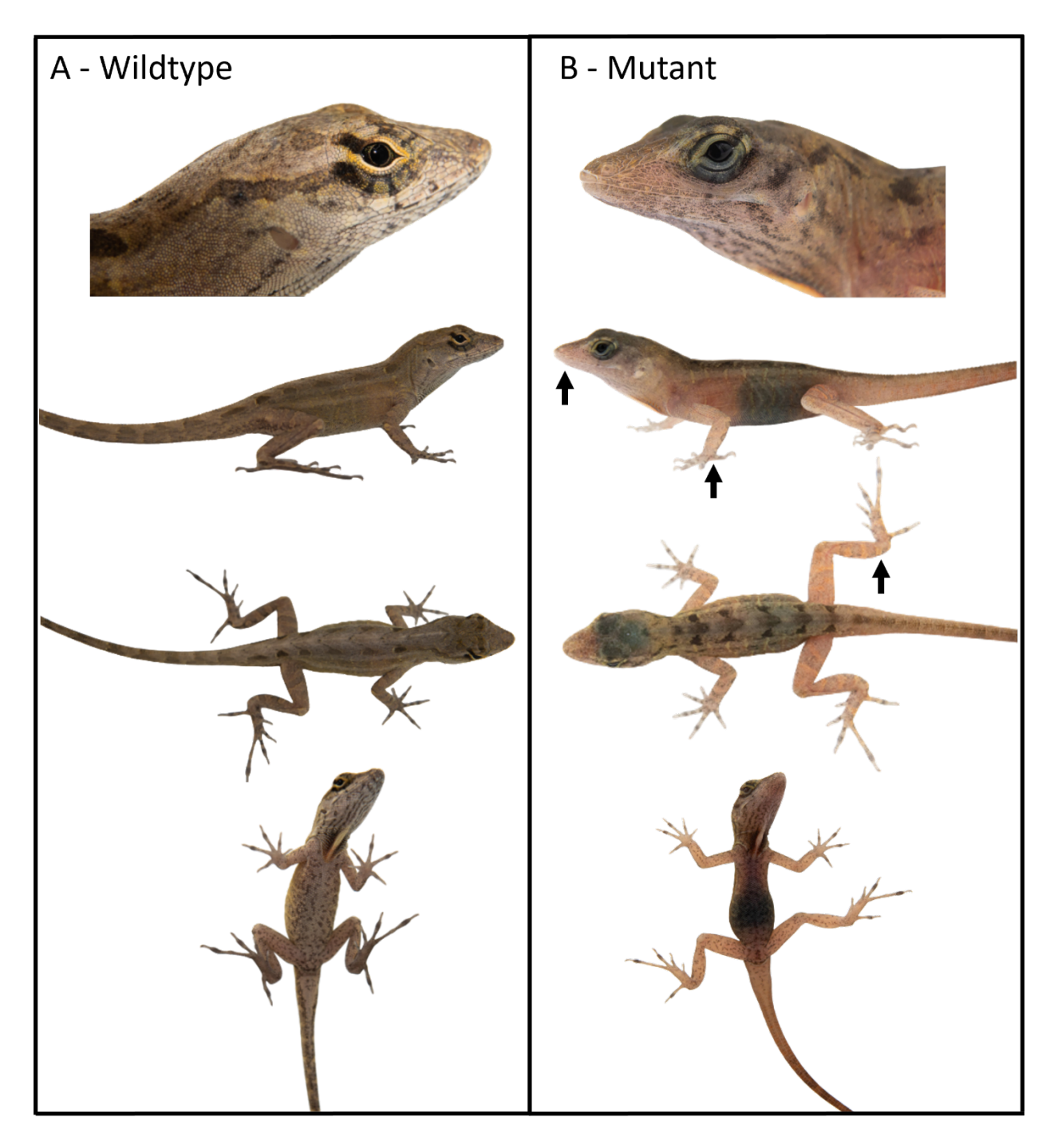


Figure 3. Phenotypic comparison between A. sagrei wild type (A) and F0 tfec mutant (B).

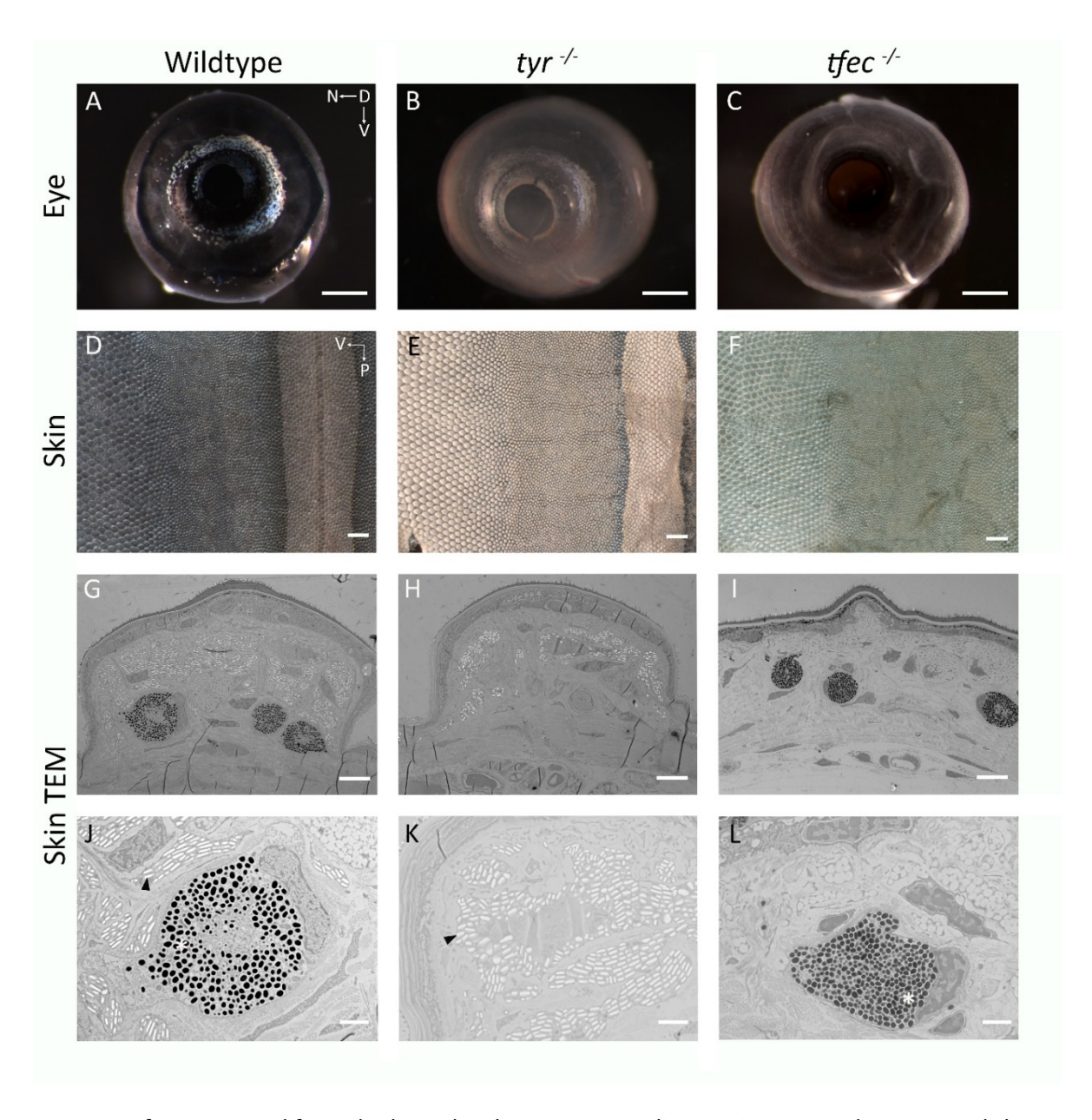


Figure 4. *Tfec* is required for iridophore development in *Anolis sagrei*. Presented are eye and skin samples from individuals having (a, d, g, j) wild-type alleles and F0 mutants with reading frame mutations in (b, e, h, k) *tyr* and (c, f, I, I) *tfec*. (a-c) anterior view of hatchling eyes. (d-f) dissected skin from trunk of hatchlings. For these panels, anterior surface is up, and the posterior surface is down. Ventral surface is on the left side of the image and the dorsal surface is on the right. The dorsal stripe can be seen on panels (d) and (e) while (f) exhibits a lack of this back pattern. (g-l) transmission electron microscopy images of individual dorsal scales (g-i) and higher magnification images of melanophores and iridophores (j-l). Melanophores hold pigmented melanosomes while iridophores reflectiveness comes from guanine crystals. For *tyr*-/- note the absence of melanosomes and the presence of guanine crystals. For *tfec*-/- note the presence of melanosomes and the absence of guanine crystals. Asterisks show melanosomes while arrowheads point to guanine crystals. Scale bars: (a-f) 500 um, (g-i) 6 um, (j-l) 2 um.

SUPPLEMENTARY FIGURES

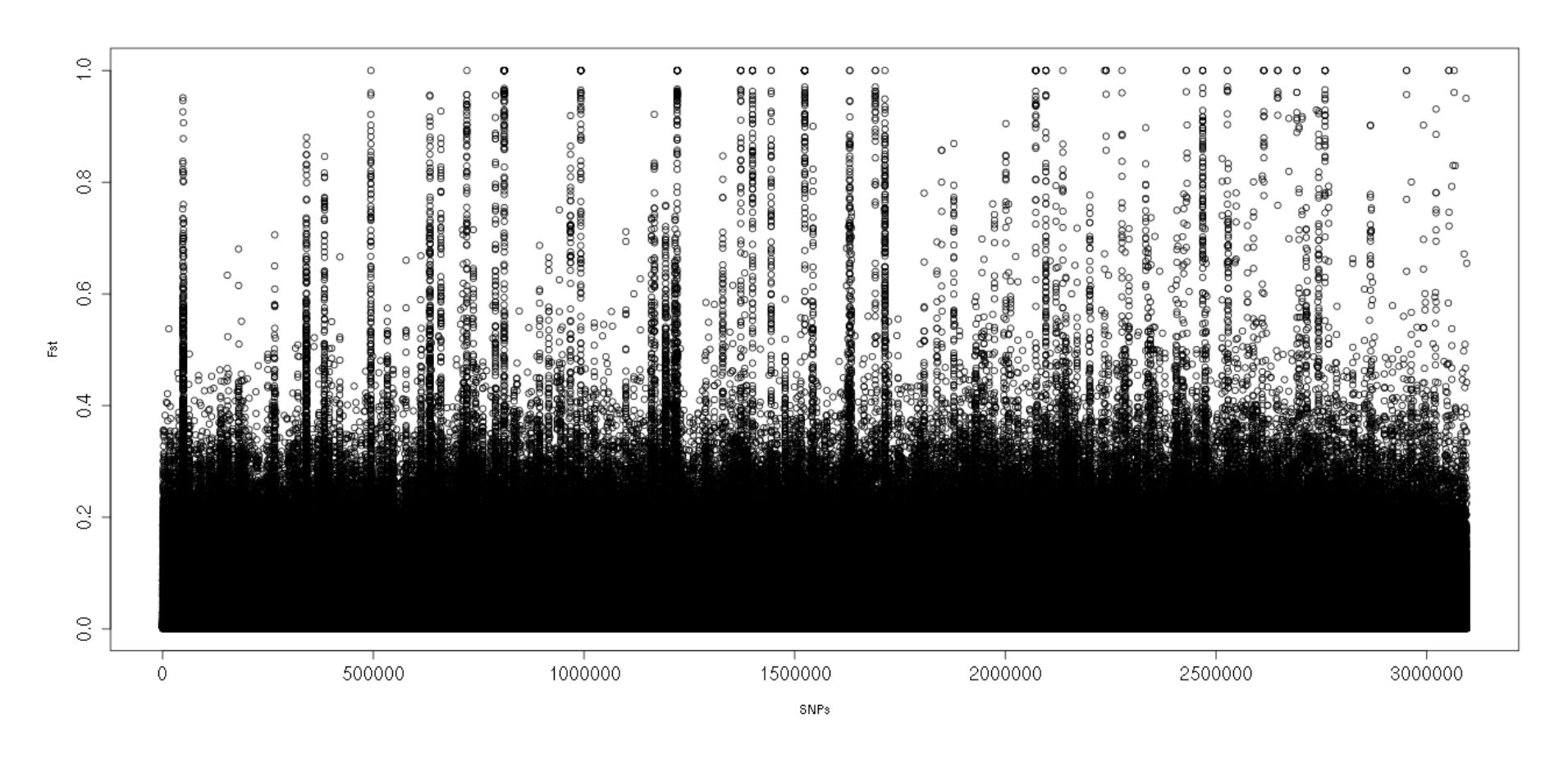


Figure S1. F_{ST} plot of piebald vs. non-piebald comparison using the fragmented draft assembly.

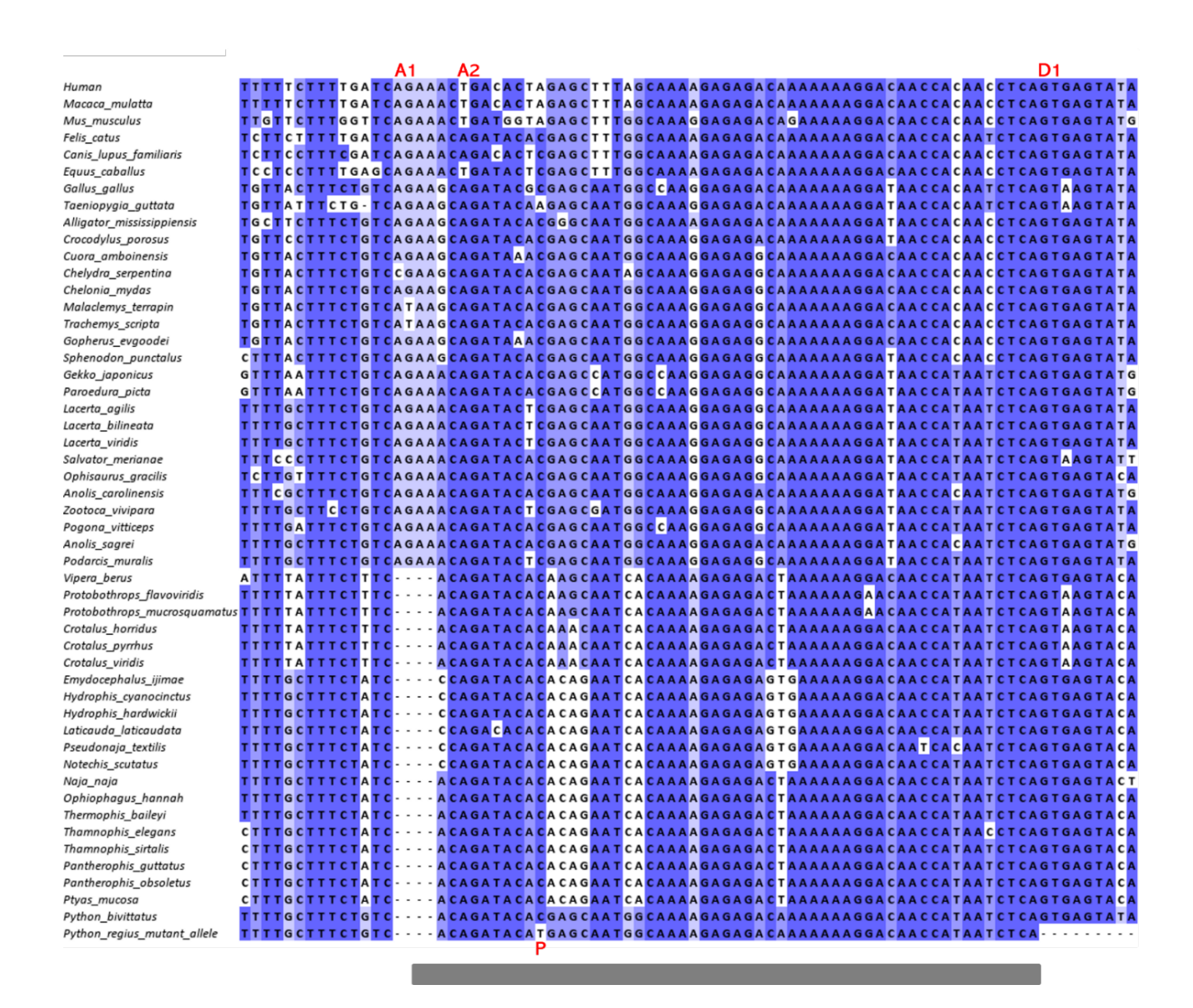


Figure S2. Multispecies (vertebrates) sequence alignment of *tfec* coding exon 5 (delineated by gray rectangle) showing nonsense mutation (P annotation). Splice acceptor sites shown by A1 and A2 annotations. Splice donor sites indicated with D1 annotation. A 4 bp deletion results in loss of A1 splice acceptor site in snakes. The alignment is coloured by percentage identity.

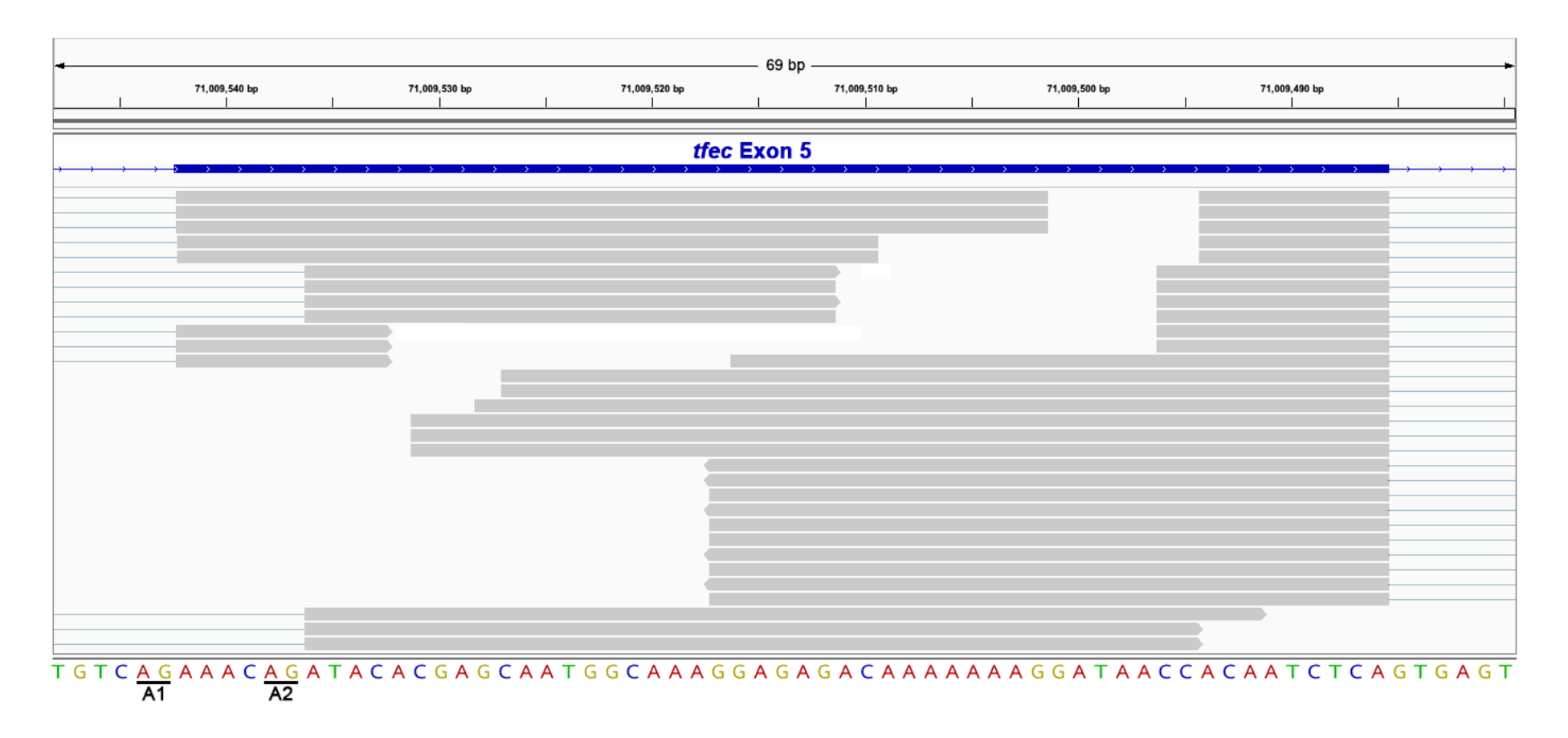


Figure S3. Alternative splicing of *tfec* exon 5 in *Anolis sagrei*. RNA-seq reads from embryonic (limbs and eyes) and adult (brain, liver, and skin) tissues of *A. sagrei* demonstrate the presence of two alternative splice acceptor sites at the 5' end of *tfec* exon 5. Blue = *tfec* exon 5, gray = individual RNA-seq reads, A1 = Acceptor site 1, A2 = Acceptor site 2.

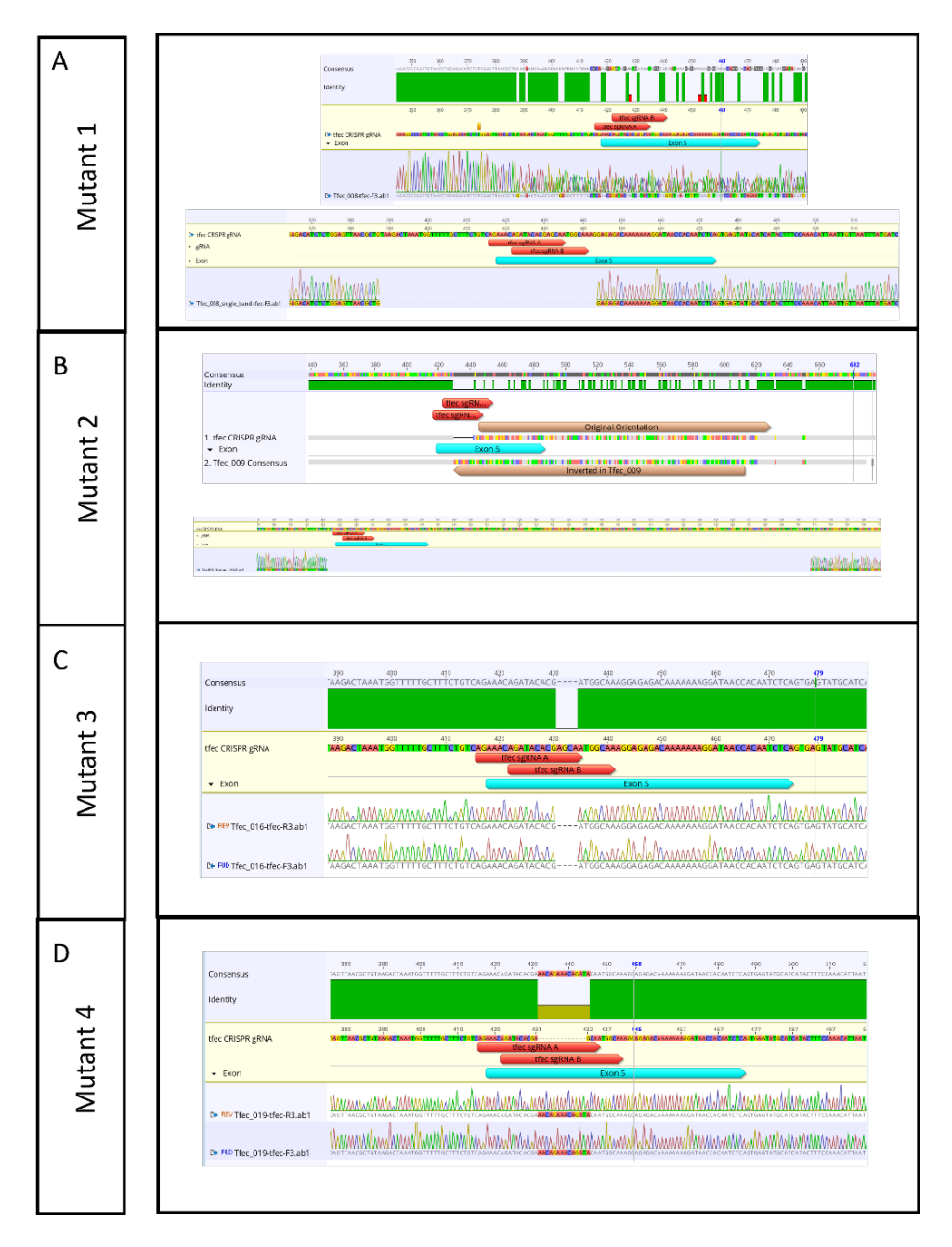


Figure S4. Chromatograms of *tfec* exon 5 from mutant *A. sagrei*. (A) Mutant 1: Overlapping signal indicates presence of multiple alleles (top panel). 56bp deletion shown in bottom panel. 1bp deletion not shown. (B) Mutant 2: Two mutant alleles detected, a local ~190bp inversion (middle panel) and a 295bp deletion (bottom panel). (C) Mutant 3: 4bp deletion. (D) Mutant 4: 13bp insertion.

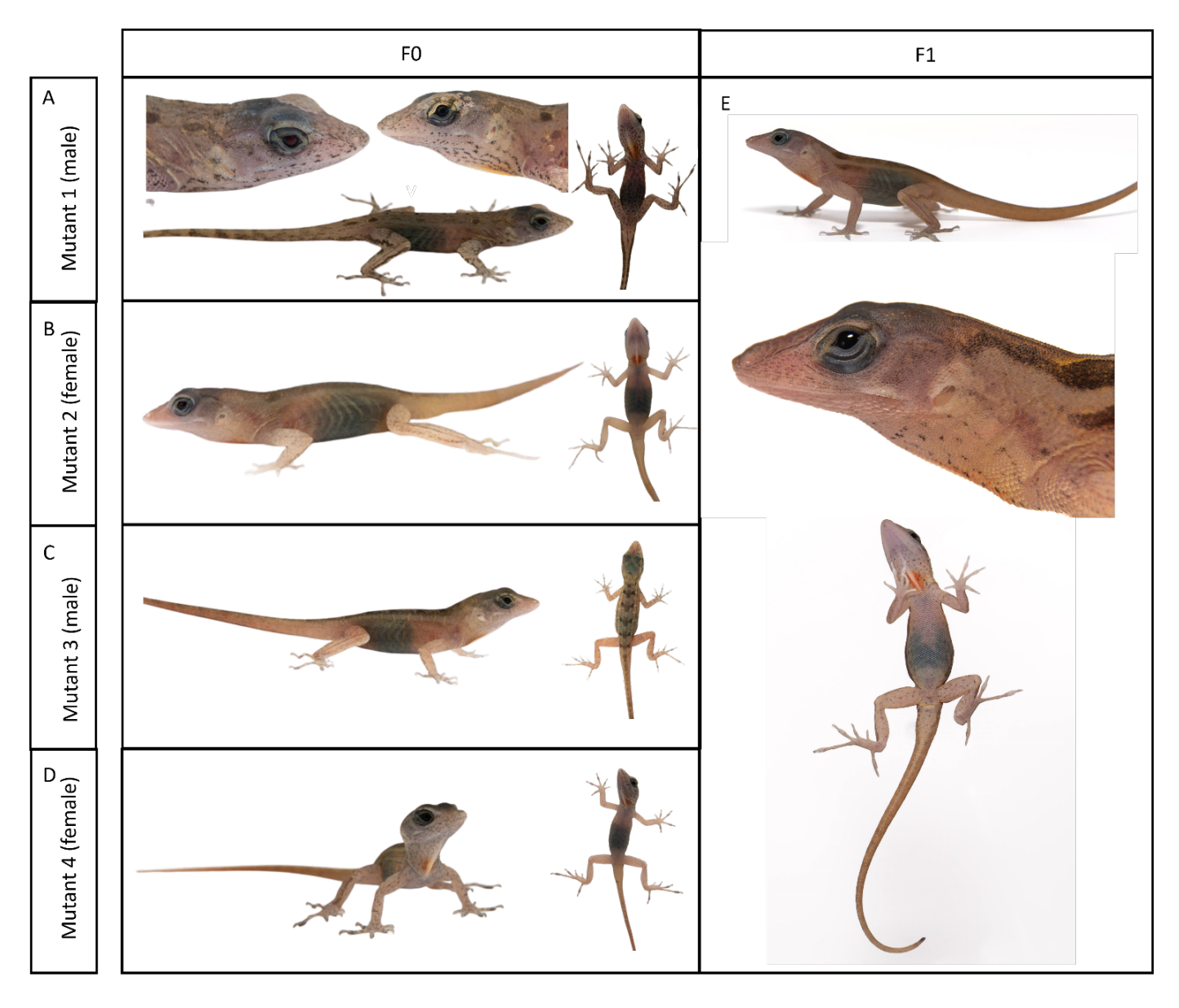


Figure S5. Mutant A. sagrei phenotypes. F0 generation: (A) Mutant 1 (male). (B) Mutant 2 (female). (C) Mutant 3 (male). (D) Mutant 4 (female). Phenotype successfully transmitted to the F1 generation.

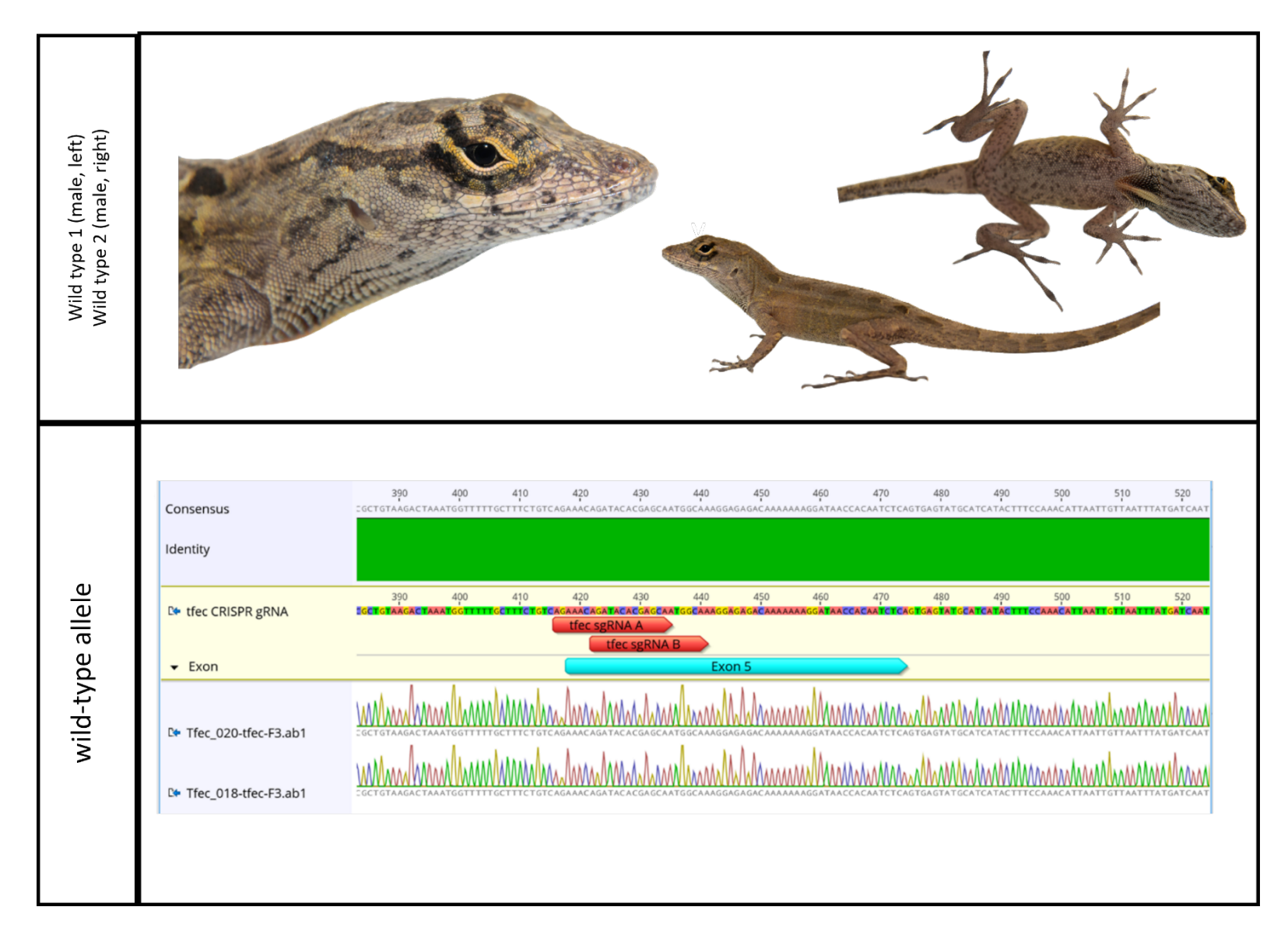


Figure S6. (top panel) Phenotypes of *A. sagrei* with normal pigmentation: wild type 1 (male, left) and wild type 2 (male, right). (bottom panel) Chromatograms: wild type 1 (bottom) and wild type 2 (top).

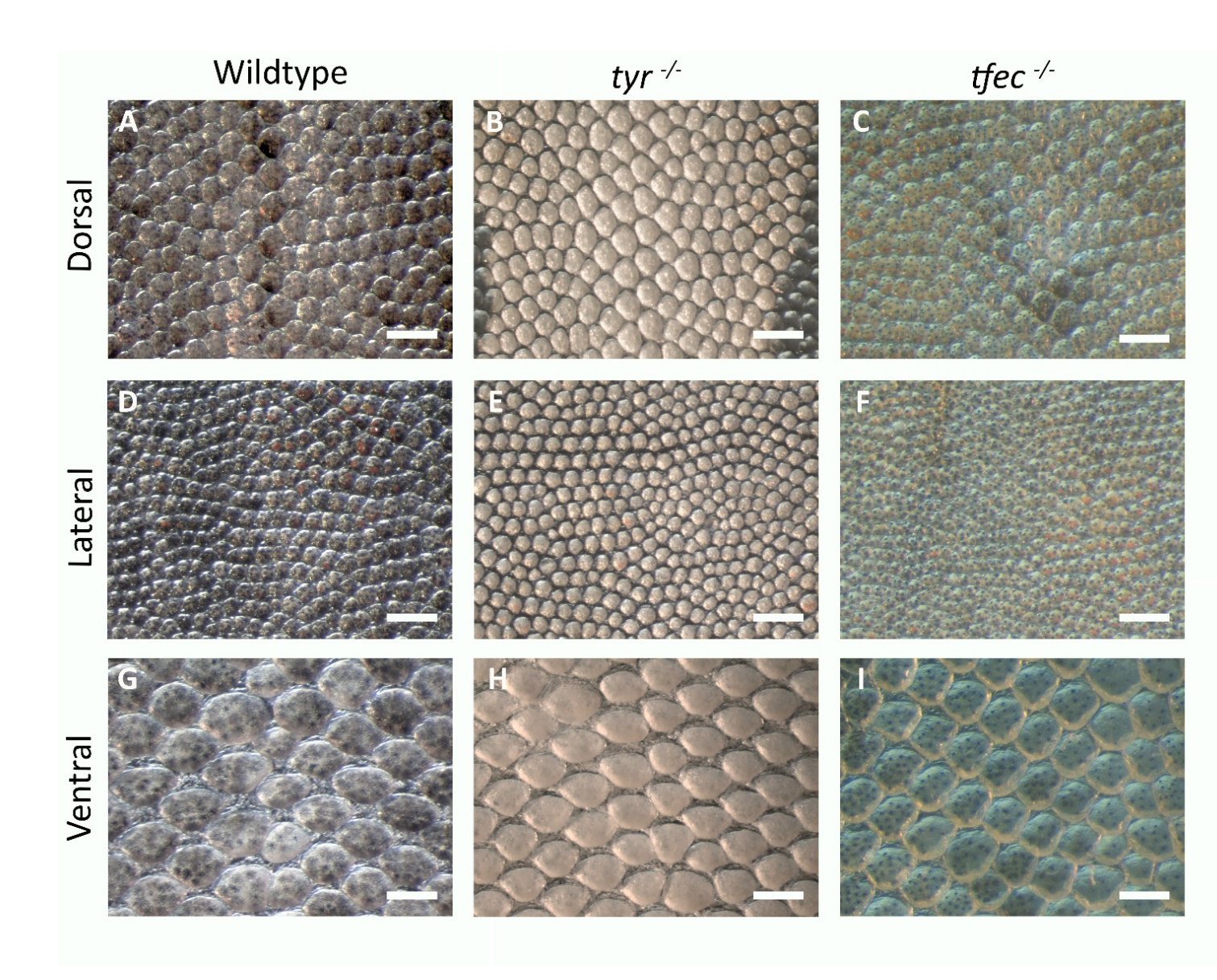


Figure S7. Close up views of *A. sagrei* skin from wild type, $tyr^{-/-}$, and $tfec^{-/-}$ hatchlings. Panels display (a,d,g) wild type, (b, e, h) tyrosinase and (c, f, i) tfec mutants. (a-c) scales along the dorsal midline. (d-f) scales along the side of the lizard. (g-i) scales along the belly of the lizard. Scale bar for all panels, 250 um. Reading frame mutations in tyr and tfec do not affect scale patterning or size but do impact coloration.